High energy density plasma science with an ultrarelativistic electron beam

C. Joshi, B. Blue, C. E. Clayton, et al.

View Online   Export Citation

ARTICLES YOU MAY BE INTERESTED IN

REVIEW PAPERS

High energy density plasma science with an ultrarelativistic electron beam[a]

C. Joshi,[b] B. Blue, C. E. Clayton, E. Dodd, C. Huang, K. A. Marsh, W. B. Mori, and S. Wang
University of California Los Angeles, Los Angeles, California 90095

M. J. Hogan, C. O'Connell, R. Siemann, and D. Watz
Stanford Linear Accelerator Center, Stanford University, Stanford, California 94309

P. Muggli, T. Katsouleas, and S. Lee
University of Southern California, Los Angeles, California 90089

An intense, high-energy electron or positron beam can have focused intensities rivaling those of today's most powerful laser beams. For example, the 5 ps (full-width, half-maximum), 50 GeV beam at the Stanford Linear Accelerator Center (SLAC) at 1 kA and focused to a 3 micron rms spot size gives intensities of $>10^{20}$ W/cm^{-2} at a repetition rate of >10 Hz. Unlike a ps or fs laser pulse which interacts with the surface of a solid target, the particle beam can readily tunnel through tens of cm of steel. However, the same particle beam can be manipulated quite effectively by a plasma that is a million times less dense than air! This is because of the incredibly strong collective fields induced in the plasma by the Coulomb force of the beam. The collective fields in turn react back onto the beam leading to many clearly observable phenomena. The beam paraticles can be: (1) Deflected leading to focusing, defocusing, or even steering of the beam; (2) undulated causing the emission of spontaneous betatron x-ray radiation and; (3) accelerated or decelerated by the plasma fields. Using the 28.5 GeV electron beam from the SLAC linac a series of experiments have been carried out that demonstrate clearly many of the above mentioned effects. The results can be compared with theoretical predictions and with two-dimensional and three-dimensional, one-to-one, particle-in-cell code simulations. These phenomena may have practical applications in future technologies including optical elements in particle beam lines, synchrotron light sources, and ultrahigh gradient accelerators. © *2002 American Institute of Physics.* [DOI: 10.1063/1.1455003]

I. INTRODUCTION

Historically, high energy density plasma science (HEDPS)[1] refers to the study of high-temperature, high-density plasmas produced by a number of different types of drivers: Lasers, ion beams, z-pinches and modestly relativistic ($\gamma < 10$) electron beams. HEDPS with an ultrarelativistic electron beam, U-REB, ($\gamma \gg 10^3$) has hitherto not been explored despite the fact that the energy density associated with such a driver can be comparable to that of the most powerful other types of drivers mentioned above that are used in HEDPS. Table I below compares, for instance, the driver parameters of a 100 TW, 30 fs laser, and the existing nominally 50 GeV electron beam at the Stanford Linear Accelerator Center (SLAC).

As can be seen from Table I, the peak intensities achieved at the focus of these two drivers for HEDPS are comparable. However, the interaction of photons and electrons as they impact a solid target is very different. Unlike a fs laser pulse, which even at these ultrahigh intensities is strongly attenuated by a thin layer of plasma formed by the photons at the target surface, the U-REB can readily tunnel through tens of cm of steel. On the other hand the interaction of both an intense laser pulse and a high current electron pulse with the plasma can be qualitatively very similar when the two propagate through a low-density plasma. In either case a significant amount of drive beam energy can be transferred to the plasma electrons making them relativistic particularly in the electron blow-out regime.[2] In the laser beam case each electron receives energy on the order $(v_0/c)^2 mc^2$ whereas in the electron beam case each electron receives $\sim (n_b/n_p)^{1/2} mc^2$ amount of energy. The symbols are defined in Table II. In this sense this is a distinctly different regime of HEDPS that has not been systematically explored until now. The main motivation for using U-REBs in the plasmas is the development of the beam-driven plasma wakefield accelerator. The focus of this research is on demonstrating accelerating gradients on the order of 1 GeV/m over a meter of

TABLE I. Physical characteristics of a state-of-the-art laser and particle beams.

	100 TW laser	50 GeV electron beam
Energy per particle (eV)	1.5	50×10^9
Pulse length (FWHM) (ps)	30×10^{-3}	5
Spot size (μm)	5	3
Energy/pulse (J)	3	150
Rep rate (Hz)	100	10–120
Peak intensity (W/cm^2)	10^{20}	10^{20}

TABLE III. Typical beam and plasma parameters used in the experiments.

Number of e^- per bunch	N	$1.8–2 \times 10^{10}$
Bunch energy	E, γ	28.5 GeV, 5.58×10^3
Bunch radius	$\sigma_r, \sigma_x, \sigma_y$	30–40 μm
Bunch length	σ_z	0.7 mm
Beam density	n_b	1.5×10^{15} cm^{-3}
Normalized emittance	$\varepsilon_{N,x}$	5×10^{-5} m-rad
Plasma density	$\varepsilon_{N,y}$	0.5×10^{-5} m-rad
Plasma length	L	1.4 m

plasma. Such large fields can only be excited over this length using an U-REB.

The physical mechanisms are quite different in the laser and the beam cases but the experimentally observable effects are similar. For instance, the laser pulse interacts with the plasma electrons via the ponderomotive force which is proportional to the gradient of the intensity, whereas the U-REB plasma interaction is via the space charge electric field of the electron beam. In the so-called ''blow-out'' regime[2] (which for laser pulses occurs when $v_0/c \gg 1$ and $k_p \sigma_r \ll 1$ and for an electron pulse occurs when $n_b \gg n_p$ and $k_p \sigma_r \ll 1$) both drivers expel all the plasma electrons [on a time scale of either ω_p^{-1} laser or ω_b^{-1} (beam)] and create an ion channel. The effect of the ion channel on the photons is relatively weak arising from the modified index of refraction of the plasma. However, that is not the case for a U-REB. The space-charge force of the ion channel can influence the electron bunch in profound ways depending on certain initial conditions. In a general sense one can observe all the same effects as one would when a charged particle interacts with an electric field: Deflection, acceleration, and radiation. In the case of an electron beam these effects can be observed as (a) focusing of the beam outside the plasma, (b) deflection or

TABLE II. Definition of parameters used in text. All other symbols are as defined in the NRL Plasma Formulary (Ref. 10).

Physical parameter	Symbol/formula
Total number of beam particles	N
Initial position of the electron	r_0
Longitudinal r.m.s. size of beam	σ_z
Transverse r.m.s. size of the beam	$\sigma_x, \sigma_y, \sigma_r$
Beam (plasma) density	$n_b(n_p)$
Laser frequency (field)	ω, E_L
Normalized electron velocity	$\beta = v/c$
Longitudinal electric field	eE
Lorentz factor of the beam	$\gamma = (1-\beta^2)^{-1/2}$
Electron beam density	$n_{b0} = N/(2\pi)^{3/2} \sigma_r^2 \sigma_z$
Electron plasma frequency	$\omega_p = (n_p e^2/\varepsilon_0 m)^{1/2}$
Beam plasma frequency	$\omega_b = (n_{b0} e^2/\varepsilon_0 m)^{1/2}$
Collisionless skin-depth	c/ω_p
Plasma wave number	$k_p = \omega_p/c = 2\pi/\lambda_p$
Normalized emittance of the beam	$\varepsilon_N = \gamma\varepsilon$
Focusing beta of the beam	$\beta_{\text{beam}} = \gamma\sigma_r^2/\varepsilon_N$
Effective wiggler strength	$a = \gamma k_\beta r_o$
Betatron frequency	$\omega_\beta = \omega_p/(2\gamma)^{1/2}$
Betatron wave number	$k_\beta = \omega_\beta/c$
Matched beam radius	$r_{bm} = (\varepsilon_N/\gamma k_p)^{1/2}$
Wake amplitude	$n_1/n = eE/m\omega_p c$
Electron oscillatory velocity	$v_0/c = eE_L/m\omega c$

steering of the beam, (c) periodic oscillations of the beam spot, (d) emission of wiggler radiation in the x-ray range, (e) deceleration of the bulk of the beam, and (f) acceleration of some beam particles in the tail of the beam. Some of these effects have been studied using lower energy relativisic electron beams propagating through plasmas,[3–6] but a systematic study of all these effects under the same experimental conditions has never been carried out to date using an U-REB. There is hope that phenomena being studied here will lead to the development of new plasma technologies including new types of lenses and kickers for future high-energy particle beam lines, plasma wigglers and undulators for the next generation of synchrotron light sources, an entirely new paradigm for building high-gradient accelerators and a new class of free electron lasers.

II. EXPERIMENTAL CONDITIONS

The experimental work discussed in this review paper was carried at SLAC as part of two experimental investigations, E157 and E162, using the U-REB at the Final Focus Test Beam (FFTB) facility. The beam parameters are shown in Table III. These do not include the effect of foils and pellicles used in the experiment.[7] Unless explicitly mentioned otherwise, these parameters were used in the various experiments.

The experimental set-up has been described in detail in Ref. 7. We will describe the apparatus briefly in this article so that the experimental data presented later can be understood easily.

Figure 1 shows the schematic of the experimental set-up. The SLAC beam with the above mentioned parameters was focused near the entrance of a lithium plasma produced by photo-ionization of a 1.4 meter long lithium vapor column by an ArF laser.[8] The beam size (σ_x, σ_y), 1 m upstream and 1 m downstream of the plasma was recorded by imaging the optical transition radiation (OTR),[9] produced by the beam, onto 16 bit charge coupled device (CCD) cameras. The electron beam exiting the plasma was bent or dispersed in the vertical or y-plane using a 5.2 m long dipole bending magnet placed 3 m from the plasma exit.

The dipole magnet provided a net dispersion of 300 MeV/mm at a 1 mm thick aerogel Cherenkov radiator placed 12 m from the plasma. The Cherenkov light was split using a beam-splitter and sent to a 16 bit CCD camera to record the time integrated beam profile or to a streak camera where it was time resolved in both planes, (x vs τ) and (y vs τ), with an ~2 ps resolution, here τ is the time measured from the center of the bunch. The forward emitted x-ray radiation
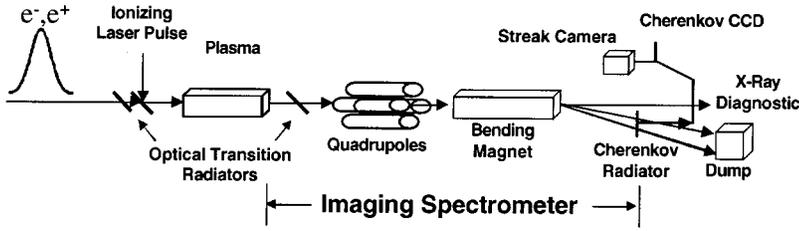
FIG. 1. The experimental set-up for studying beam-plasma interaction effects with a 28.5 GeV electron or positron beam that was used in most of the experiments described in the text. The detection set-up for x-rays in the forward direction is not shown.

from the plasma was reflected using a Si(111) crystal and recorded using two surface barrier detectors. The electron beam position downstream of the plasma was measured by a series of stripline beam position monitors (BPMs).

III. HIGH ENERGY DENSITY PLASMA SCIENCE (HEDPS) IN BEAM–PLASMA INTERACTION

The electron beam has a Gaussian profile in both transverse and longitudinal directions given by

$$n_b(x,y,z) = n_{b0} e^{-x^2/2\sigma_x^2} e^{-y^2/2\sigma_y^2} e^{-z^2/2\sigma_z^2}, \tag{1}$$

where for a round beam the total number of beam particles is given by

$$N = \int_{z=-\infty}^{\infty} \int_{r=0}^{\infty} n_b(x,y,z) 2\pi r \, dr \, dz, \tag{2}$$

from which we obtain the peak beam density as

$$n_{b0} = \frac{N}{(2\pi)^{3/2} \sigma_r^2 \sigma_z}. \tag{3}$$

It is well-known that for a relativistic beam the radial space charge force and the self-magnetic force counter and cancel each other to the order $1/\gamma^2$.[11] Thus an initially collimated U-REB propagates in vacuum with an expanding envelope due mainly to its intrinsic emittance.

When such a beam is injected into a plasma, the plasma electrons begin to be expelled from a region surrounding the beam in order to preserve the charge neutrality of the plasma. This in turn perturbs the balance between the self-forces of the beam mentioned above. What then happens to the beam depends on the relative beam and plasma parameters. If $n_p > n_b$ and $k_p \sigma_r \ll 1$, the beam is self-pinched by its own magnetic field.[12] On the other hand if $n_b > n_p$, known as the underdense plasma condition, the beam electrons blow out the plasma electrons leaving behind an ion column.[13] The ion column in turn exerts a focusing force on the beam. It is this latter regime of propagation, known as the ion focused regime that is of interest to this work.

The formation of the ion channel and the action of the ion channel back on the beam are both transient effects for beams that are both narrow, $k_p \sigma_r \ll 1$, and short $k_p \sigma_z \sim 0(1)$. Nevertheless, the radius of the ion channel that is formed can be estimated by equating the space-charge field of the beam and the electrostatic field of the ion column at this radius[14] leading to

$$r_i = \sigma_r \left(\frac{n_{b0}}{n_p} \right)^{1/2}. \tag{4}$$

For $n_{b0} \gg n_p$, plasma electrons are blown out from a region of plasma that is much wider than the beam spot size.

There are now a number of physical effects that ensue as the ion channel exerts a focusing force on the electron beam. The radial electrostatic field of this ion[15] channel is given by

$$E_r = \frac{1}{2} \frac{n_p e}{\varepsilon_0} r, \tag{5}$$

which varies linearly with r. Substituting $r = \sigma_r$ leads to

$$E_r = 9 \times 10^{-15} n_p [\text{cm}^{-3}] \, \sigma_r [\mu\text{m}] \, \text{MV/m}. \tag{6}$$

This radial electric field has profound transverse and longitudinal effects on the beam which we will discuss. Of particular interest is the case when $k_p \sigma_z \sim 0(1)$, for which a strong longitudinal electric field is excited behind the head of the beam.

A. Beam focusing or underdense plasma lensing

It can be seen from Eq. (5) that in the underdense regime, the ion column exerts a focusing force that increases with r and, therefore, a section of plasma acting as a focusing lens has, in principle, no spherical aberrations. However such a lens still has longitudinal and chromatic aberrations. Spherical aberrations are caused by the time dependence of ion channel formation whereas the chromatic aberrations arise from the energy variations within the beam. The effective focusing gradient can be found from Eq. (1) as

$$B_\theta/r = 3 \times 10^{-9} n_p [\text{cm}^{-3}] \, \text{G/cm}. \tag{7}$$

In the thin lens approximation the electron beam after traversing a length L of an ion column with density n_p will focus at[16]

$$f = \frac{2\gamma c^2}{L\omega_p^2} = 5.6 \times 10^{11} \frac{\gamma}{L(\text{cm}) n_p (\text{cm}^{-3})}. \tag{8}$$

As an example, using Eqs. (7) and (8) a 10 cm long, 10^{15} cm^{-3} density plasma lens will have a focusing gradient of 3 MG/cm and will focus a 50 GeV SLAC beam in just 8.6 cm.

Consider the case of a beam of emittance ε focused to a spot size σ_0^* at a distance s_0 away. The initial beam β is related to the beam beta at the waist ($\beta_0^* = \sigma_0^*/c$) by

$$\beta = \beta_0^* \left(1 + \frac{s_0^2}{\beta_0^{*2}} \right). \tag{9}$$

When the beam traverses a thick lens of length L ($L \ll s_0$) and density n_p, the beam beta at the lens exit is given by

TABLE IV. Plasma lens characteristics for three incident spot sizes.

Initial spot size		Final spot size		Focal length		
σ_o^* (μm)	n_b/n_p	σ_x^* (μm)	σ_y^* (μm)	f_x (μm)	f_y (μm)	$(c/\omega_{pb})/\sigma_z$
50	4	6	1.5	24.4	24.7	0.24
40	6.5	7.4	1.9	23.8	24.7	0.19
30	11	9.6	2.5	22.2	24.6	0.14

$$\beta_L = \frac{\beta_0}{2} + \frac{1}{2K\beta_0^*} + \left(\frac{\beta_0}{2} - \frac{1}{2K\beta_0^*}\right)\cos(2\sqrt{K}L)$$

$$- \frac{2s_0}{2\sqrt{K}\beta_0^*}\sin(2\sqrt{K}L), \tag{10}$$

where $K = \omega_p^2/2\gamma c^2$. The beam beta at the new waist is given by[17]

$$\beta^* = \frac{\beta_0^*}{1 + K(\beta_0 - \beta^*)\beta_0^*} \tag{11}$$

and the new waist is located at a distance s from the lens entrance given by

$$s = (\beta^*(\beta_L - \beta^*))^{1/2}. \tag{12}$$

The demagnification ratio defined as $\sigma_0^*/\sigma^* = (\beta_0^*/\beta^*)^{1/2}$ can be maximized with respect to σ_0^*, n_p, and L. Table IV illustrates the effect of varying the initial spot size σ_0^* on the final spot size σ^*. Plasma parameters were: $n_p = 1.2 \times 10^{14}$

FIG. 3. Physical mechanism for collective "refraction" of a relativistic electron beam traversing a plasma/neutral gas boundary: (a) Side view and (b) front view of beam and plasma illustrating how asymmetric blowout creates a net deflection force F.

cm^{-3}, $L = 10$ cm. The beam parameters were: $N = 2 \times 10^{10}$ electrons, $\sigma_z = 1$ mm, $\varepsilon_{Nx} = 60$ mm-mrad, and $\varepsilon_{Ny} = 15$ mm-mrad. As σ_0^* is decreased, the n_b/n_p ratio increases causing the blow-out to be reached earlier in the bunch. The longitudinal aberrations are thereby reduced. However, as σ_0^* is decreased the minimum spot size increases because of the beam emittance contribution to σ^* in these examples. Note that the focal length of the lens is relatively independent of σ_0^*, and that the values of σ^* are different in the x and y planes because $\varepsilon_{Nx} \neq \varepsilon_{Ny}$.

The predictions of the analytical theory have been tested using the 3D quasi-state, particle-in-cell (PIC) code QUICKPIC.[18] The initial beam and plasma parameters are those of the $\sigma_0^* = 50$ μm case in Table IV. Figure 2 shows that the spot sizes at the beam waist located 25 cm downstream of the lens exit are $\sigma_x^* = 5$ μm and $\sigma_y^* = 2$ μm, respectively. These values are in excellent agreement with those obtained from the analytical model (Table IV). The choice of n_p and σ_z in this example is such that $k_p\sigma_z \cong \sqrt{2}$, therefore, the plasma electrons thus rush back on axis in the back of the electron bunch. They create a defocusing force that causes $\sigma_{x,y}^*$ to blow up in the back of the bunch (position > 2300 μm on Fig. 2).
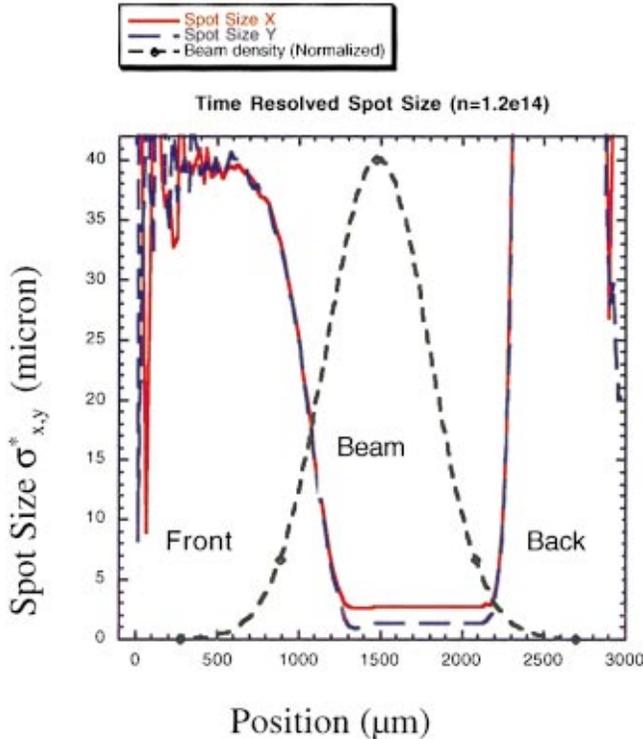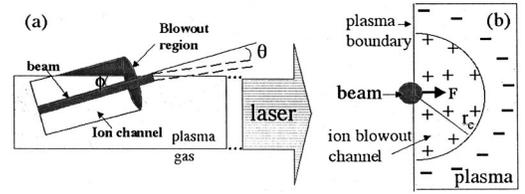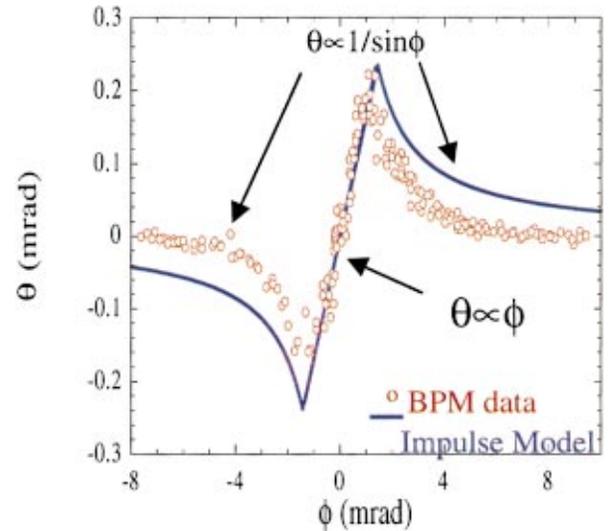

FIG. 2. (Color) Simulation results from code QUICKPIC showing time dependent focusing for a 28.5 GeV beam after traversing a 10 cm long, 1.2 $\times 10^{14}$ cm^{-3} plasma at 25 cm from the plasma exit in both x and y transverse directions. The beam waist is placed at the plasma entrance.

FIG. 4. (Color) A plot of beam deflection angle θ measured with a beam position monitor versus angle between the ionizing laser and the beam ϕ. ϕ is also the angle between the beam and the plasma. For incident angles ϕ less than 1.2 mrad the beam appears to be internally reflected. The solid line is the prediction of the simple impulse model described in the text.

In the above examples the demagnification factors are between 10 and 25. Plasma lenses with large demagnification factors will be highly desirable for increasing the luminosity in future linear colliders. However, the penalty for doing so may be a significant synchrotron energy loss resulting in background problems at the detector.

B. Collective refraction of the beam

If the electron beam is propagated at an angle ϕ with respect to the axis of the plasma column such that it encounters a plasma–vacuum or a plasma–neutral gas boundary, it can experience a deflection which can be thought of as a collective refraction effect. Under certain conditions the beam is not only refracted away from the normal it can actually be totally internally reflected as a photon beam would do in an optical fiber. As discussed above, when the beam is fully inside the plasma, the head of the beam expels the plasma electrons out to a radius r_i. As the beam approaches the plasma-gas boundary the ion channel becomes asymmetric as shown in Figs. 3(a) and 3(b). This causes the beam to be deflected towards the plasma.

The magnitude of this deflection has been estimated using an impulse model.[19] As the beam approaches the plasma–neutral gas boundary at an angle ϕ, the force on the beam due to the ion channel of radius r_i is given by Gauss's law as

$$F = -2n_p e^2 r_i.$$

The beam spends roughly $2r_i/c \sin \phi$ amount of time near the edge. The impulse on the beam is thus the Coulomb force multiplied by the time that the beam resides within the ion channel. Dividing by the beam's parallel momentum γmc gives a scaling law for the deflection angle θ, valid for $\phi > \theta$ as

$$\theta = \frac{8}{\pi} \frac{\alpha N r_e}{\sqrt{2\pi} \gamma \sigma_z \sin \phi}, \tag{13}$$

where $eN/\sqrt{2\pi}\sigma_z$ is the charge per unit length of the beam and α is a numerical factor which is <2 for beams that are longer than λ_p.

The impulse model breaks down at small angles of incidence ϕ such that the deflection angle θ is on the order of ϕ. In this case the beam can be totally internally reflected. This is a collective refraction effect whose magnitude in a rather dilute plasma of density $\sim 10^{14}$ cm^{-3} (typically $\phi < 1$ mrad as will be seen later) can be orders of magnitude greater than that expected from single electron considerations.

We have experimentally demonstrated this "refraction" effect by deliberately propagating the electron beam at an angle ϕ with respect to the plama column. Figure 4(a) shows the actual electron–beam deflection (circles) measured using a BPM and the theoretical deflection (solid line) as a function of ϕ. $\phi = 0$ degrees means that the U-REB and the ionizing laser are exactly co-propagating. By varying the angle the laser makes with respect to the electrons, the electron beam can be made to exit from either side of the plasma column. When the angle of deflection θ is plotted against the incident angle ϕ, this gives to a symmetric curve about θ

$=0$ degrees. For incident angles up to 1.2 mrad the deflection is seen to be proportional to $1/\sin \phi$ as predicted. However, for $\phi < 1.2$ mrad the beam appears to be totally internally reflected, i.e., $\theta \propto \phi$, again in good agreement with the theoretical model. It is remarkable that a 28.5 GeV beam that is able to tunnel through several centimeters of steel is totally internally reflected, by collective fields of plasma that is roughly million times less dense than air.

C. Betatron oscillations of the beam envelope

If the density length product of the plasma is large enough, the electron beam can focus within the plasma itself. As the plasma density is further increased the electron beam can undergo multiple betatron oscillations inside the plasma.[20] The behavior of the electron beam with a normalized emittance ε_N is described by the beam envelope equation

$$\sigma_r''(z) + \left[K^2 - \frac{\varepsilon_N^2}{\gamma^2 \sigma_r^4(z)}\right] \sigma_r(z) = 0, \tag{14}$$

where $K = \omega_p / (2\gamma)^{1/2} c$ is the restoring constant of the plasma or equivalently the betatron wave number k_β. The beam is said to be matched to the plasma if $\beta_{\text{beam}} = 1/K = \beta_{\text{plasma}}$. In this case the beam radius remains constant as the beam propagates through the plasma. This matched beam radius r_{bm} is found by letting $\sigma''(z) = 0$ in Eq. (12) giving $r_{bm} = (\varepsilon_N / \gamma k_p)^{1/2}$. If the initial beam radius is larger than r_{bm} then the beam *envelope* oscillates with a spatial period π/K which is equal to half the individual particles' betatron wavelength. The beam particles exit the plasma with a well defined deflection angle

$$\sigma_r' = \sigma_r k_\beta |\sin k_\beta z|. \tag{15}$$

The phase advance experienced by the beam envelope in a plasma of density n_p and length L is

$$\Psi_L(n_p) = \int_0^L K dz = K(n_p)L \ \alpha \ n_p^{1/2}. \tag{16}$$

It is clear that whenever $\Psi_L(n_p) = m\pi$ radian the beam size at the exit of the plasma will be the same as the beam size at the entrance of the plasma. At these values of phase advance the exit angle is zero for a beam that is focused to a waist at the plasma entrance, and therefore, the beam is transparent to the plasma. On the other hand, whenever $\Psi_L(n_p) = (m+1)\pi/2$ radian the beam exits the plasma at a focus and with a maximum divergence angle which scales as k_β or $\sqrt{n_p}$.

The above discussion is strictly valid for the steady state propagation of a beam in a preformed ion channel. If the ion channel is induced by the beam itself which has a finite rise-time, different longitudinal slices of the beam can undergo different number of betatron oscillations in a plasma with a given product $n_p L$. However, if $n_{b0} > n_p$ most of the beam can be affected by the ion channel that is fully denuded of plasma electrons. Thus, the envelope equation can be used to compare experiments with theory. In the experiment the beam spot size cannot be measured inside the plasma. It is usually measured at some distance outside of the plasma as

FIG. 6. Exit angle of a 28.5 GeV beam after traversing a 1.4 m long plasma whose density is being increased. The solid curve is the prediction of the theory, Eq. (15). The peaks angles increase as k_β or $\sqrt{n_p}$ as shown by the solid parabola.
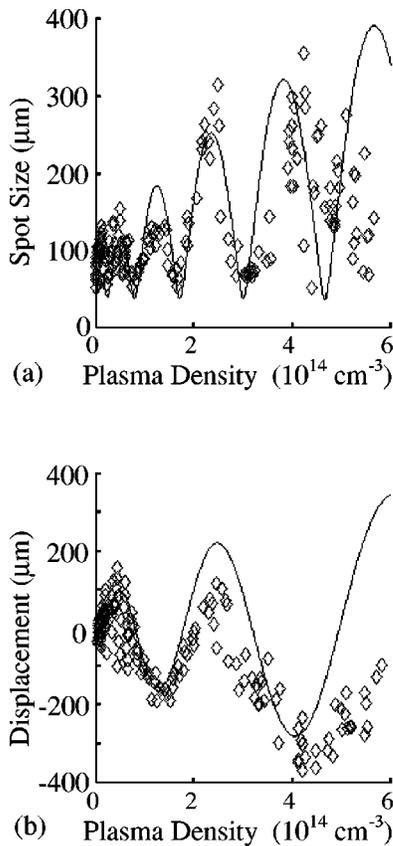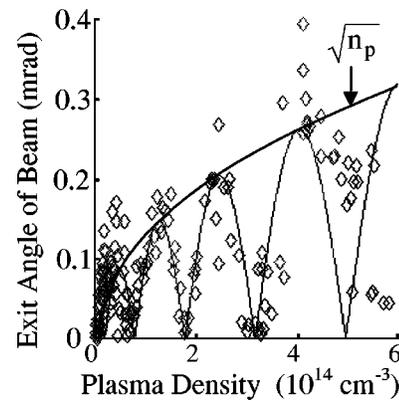

FIG. 5. (a) Multiple oscillations of the spot-size due to betatron motion of a 28.5 GeV electron beam in a 1.4 m long lithium plasma as the plasma density is increased. The solid line is a theory fit to the measured data using the beam envelope equation, Eq. (14). (b) Centroid oscillations of a 28.5 GeV electron beam measured using the downstream OTR detector as a function of plasma density. Solid line is the prediction of the envelope equation, Eq. (14) with $\varepsilon_N = 0$.

the plasma density, and therefore, Ψ_L is varied. The measured spot size can thus be compared as a function of Ψ_L using Eq. (14).

In recent experiments (with beam parameters given in Table III) multiple, betatron oscillations of the beam inside the plasma are clearly inferred from oscillations of the spot size of the beam as observed 1 m downstream of the plasma by imaging the optical transition radiation (OTR)[20] produced by the electron beam as it traverses a 25 μm thick titanium radiator placed at 45° with respect to the beam axis. Typical experimental data are shown in Fig. 5 where the plasma density is increased from 0 to 6×10^{14} cm^{-3}. The spot size of the beam is seen to oscillate at approximately twice the betatron frequency as expected. The beam envelope equation (solid line in Fig. 5) predicts the densities where the spot size minima and the spot size maxima occur up to a density of $\sim 3 \times 10^{14}$ cm^{-3}. Beyond this, the beam is too long ($k_p \sigma_z < \sqrt{2}$) and n_{bo} becomes comparable to n_p. Therefore, the beam behavior is not well described by the envelope equation [Eq. (14)] where the focusing force is due to a pure ion channel.

In addition to the multiple oscillations of the overall beam envelope which occurs when an unmatched beam is sent into a plasma, the beam centroid (or center-of-mass of the beam) can also oscillate about the ion channel axis but at half the frequency of the envelope oscillation frequency. These centroid oscillations occur because the U-REB from a linear accelerator typically has a head-to-tail transverse tilt. The axis of the ion channel is defined by the head of the beam. This means that the bulk of the beam charge has an initial transverse offset with respect to the axis of the ion channel. This causes the beam centroid to oscillate about the axis at the betatron frequency. This oscillation can be quantified by measuring the position of the beam centroid downstream of the plasma using the OTR diagnostic. We have clearly observed these oscillations in our experiments [see Fig. 5(b)]. Again, the simple theory [Eq. (14)] with $\varepsilon_N = 0$ is able to predict the values of the plasma density where the beam returns to its original undeflected position as well as the actual magnitude of the deflection fairly well.

We have also plotted the exit angle σ' of the beam as a function of plasma density measured from the beam trajectory using 3 BPMs placed downstream of the plasma. This is shown in Fig. 6. One can see that the magnitude of the maximum exit angle scales as k_β or $\sqrt{n_p}$, Eq. (15) as manifested by sloshing of the bulk of the electrons in the ion channel.

D. The electron hosing instability

The transverse effects discussed so far are all zeroth order effects. Even though the electron beam is typically a few c/ω_p long, there is one transverse instability that is of concern to the stable propagation of the electron beam: the electron hosing instability.[21] The electron housing instability can lead to the growth of transverse perturbations on the beam due to the nonlinear coupling of the beam electrons to the plasma electrons at the edge of the ion channel through which the beam propagates.[21–23] As a result of this coupling these perturbations can grow nonlinearly leading to, in the worst scenario, the transverse break-up of the beam.

The differential equations that describe the coupling between the centroid offset of the beam slice x_b and the centroid offset of the preformed ion channel x_c at a position ξ within the beam are

Phys. Plasmas, Vol. 9, No. 5, May 2002

High energy density plasma science . . .   1851

$$\partial^2 x_b + k_\beta^2 x_b = k_\beta^2 x_c,$$

$$\partial^2 x_c + \omega_0^2 x_c = \omega_0^2 x_b, \tag{17}$$

where $\xi = z/c - t$, $s = z$ and $\omega_0 = \omega_p/\sqrt{2}$. These equations can be numerically solved to calculate the growth of a particular beam slice at ξ after it has traversed a distance s in the plasma. However, in the asymptotic limit, the displacement $x_b(s, \xi)$ of the longitudinal slice of the beam with an initial linear head-to-tail tilt x_0 is given by[13]

$$x_b(s, \xi) = 0.341 \frac{x_0(\xi)}{A^{3/2}} e^A \cos\left\{ k_\beta s - \frac{A}{\sqrt{3}} + \frac{\pi}{12} \right\}, \tag{18}$$

where the factor

$$A = \frac{3^{3/2}}{4} [(k_\beta s)(\omega_0 \xi)^2]^{1/3}. \tag{19}$$

For beam parameters given in Table I, Eq. (18) predicts that there can be a factor 6 growth of a slice placed at $\xi = 5$ ps as it propagates through a meter long, 2×10^{14} cm^{-3} density plasma.

The above estimates raise a serious issue about the ability to propagate U-REB over long distances in dense plasmas. However, it should be noted that the theory assumes that a pre-formed channel with a constant radius exists whereas in many experimental situations the dynamically formed ion channel has a longitudinally varying radius. The theory also neglects longitudinal dynamics (see later) of the plasma electrons and nonideal experimental factors such as asymmetric beams and longitudinal density gradients. All these factors tend to suppress the hosing growth.

Using OSIRIS[24] we have carried out 3D, one-to-one PIC code simulations to study hosing when an U-REB propagates through long dense plasmas.[25] The physical dimensions of the system were $(17.6 \times 4 \times 4)c/\omega_p$ at a density of 1.7×10^{14} cm^{-3}. The beam had a Gaussian shape with $\sigma_z = 0.63$ mm, $\sigma_r = 40$ μm, $\varepsilon_N = 15$ mm-mrad, $Q = 3.4$ nC, and $\gamma = 6 \times 10^4$. These parameters are very close to the experimental beam parameters of Table III. The initial tilt on the beam was modeled using experimental data[25] as shown in Fig. 7(a). Figure 7(b) shows oscillations of two slices of the beam inside the plasma. The dotted line is the transverse motion of a 0.1 ps wide slice at the center of the beam. The bold line is the oscillation of a second 0.1 ps wide slice 5 ps behind the center slice. The dashed line is the behavior of the same slice obtained from numerical integration of Eq. (17) which predicts a growth factor of about 5 after 1.2 m propagation through the plasma. There appears to be some amplification of the offset of the slice at 5 ps as the beam propagates through the plasma. However, the amplification factor is about half of the theoreically predicted growth (dashed line).

Measurements are currently underway to check if this reduced growth rate seen in simulations indeed helps stable propagation of the electron beam in practice. These will be reported elsewhere.
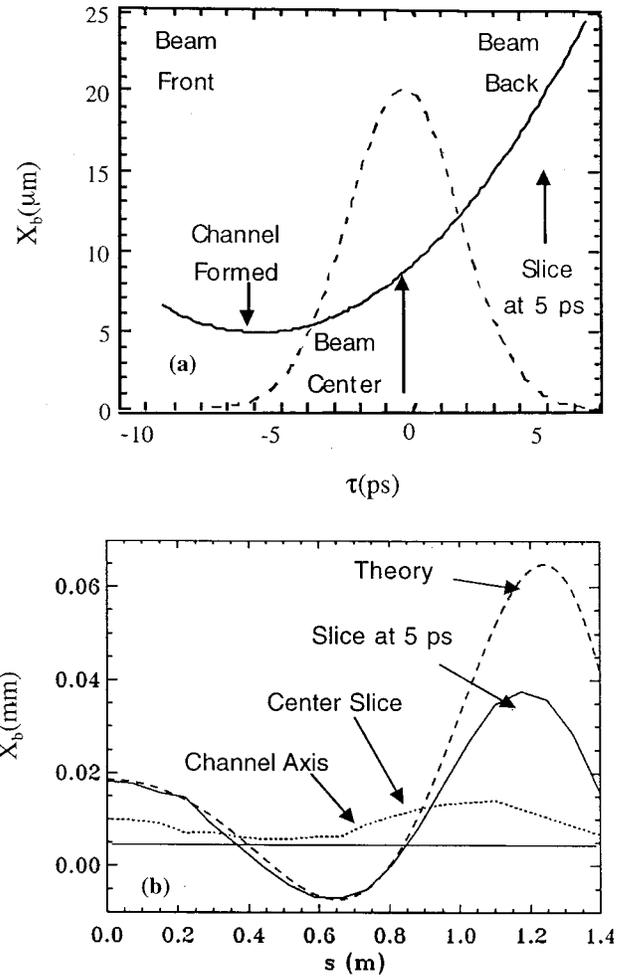

FIG. 7. (a) The longitudinal shape of the beam used in the OSIRIS simulations of electron housing. The axis of the ion channel is defined by $\tau = -5$ ps. (b) Results on growth of the transverse displacement of two slices of the beam due to the electron-hosing instability as the beam propagates through a 1.7×10^{14} cm^{-3}, 1.4 m long plasma using the 3D, PIC code OSIRIS. Also shown is the theoretically expected growth rate (dotted line) for the $\tau = 5$ ps slice using Eq. (18).

E. Emission of betatron radiation

There is a very important, observable consequence of betatron motion of electrons in a long ion column. It is the emission of betatron radiation in a narrow cone angle in the forward direction. This can be understood easily in the following way: Consider the motion of a single electron with an initial transverse displacement r_0 from the axis of the ion channel

$$\mathbf{r} = \mathbf{r}_0 \cos \phi,$$

$$\boldsymbol{\beta}_r = -\mathbf{r}_0 k_\beta \sin \phi, \tag{20}$$

$$\dot{\boldsymbol{\beta}}_r = -\mathbf{r}_0 k_\beta \omega_\beta \cos \phi \quad \text{with} \quad \frac{d\phi}{dt} = \omega_\beta.$$

As a result of this periodic acceleration the electron radiates betatron (synchrotron) radiation. The total radiation power is given by[26]
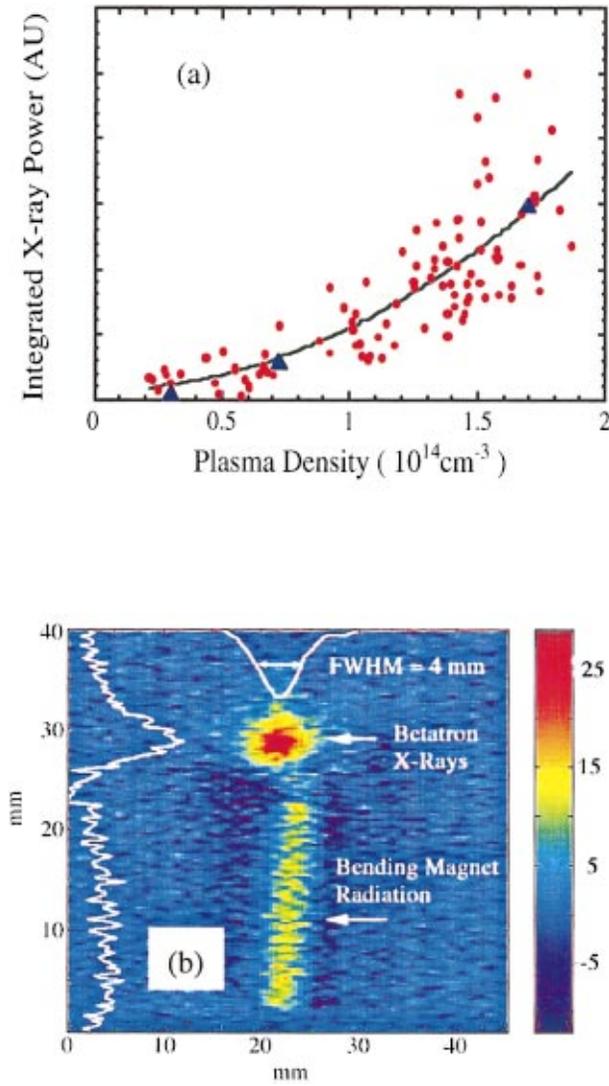
FIG. 8. (Color) (a) The estimated (triangles) and the measured (dots) x-ray energy in the 5–30 keV range as a function of plasma density. The solid line is a quadratic fit to the data. (b) Processed image produced on a fluorescent screen as recorded by a CCD camera showing the betatron x-rays produced by the plasma $n_p = 2 \times 10^{13}$ cm^{-3} (circle at the top) and a vertical stripe of remnant synchrotron radiation produced by a dipole bend magnet.

$$P(t) = \frac{2e^2\gamma^2}{3m^2c^3}[\dot{\mathbf{P}}^2 - m^2c^2\gamma^2] \cong \frac{2e^2\gamma^2\dot{\mathbf{P}}_r^2}{3m^2c^3}, \tag{21}$$

where $\mathbf{P}_r = \gamma mc\boldsymbol{\beta}_r$. Substituting for $\dot{\boldsymbol{\beta}}_r$ one can see that the total radiated power is proportional to ω_β^4 which scales as n_p^2. The radiation is emitted in a narrow cone angle in the direction of the propagation of the beam. This angle is $\sim \alpha/\gamma$ where α is the effective wiggler strength given by $\alpha = \gamma k_\beta r_0$ which for U-REB can be $\gg 1$. The spectrum of this betatron radiation has resonance frequencies[27] at

$$\omega_r = \frac{2m\gamma^2\omega_\beta}{[1 + \alpha^2/2 + (\gamma\Omega)^2]}, \tag{22}$$

where m is the harmonic number and $\Omega \ll 1$ is the typical observation angle from the beam axis. In an electron beam, each electron has a different r_0 and, therefore, α which leads to broadening of the spectrum. The rate at which a single

electron loses energy due to radiation is simply $\langle P \rangle/c$. Substituting for $\mathbf{P}_r$ and averaging over one betatron period one obtains

$$W_{\text{loss}} = \frac{\langle P \rangle}{c} = \frac{1}{3} r_e mc^2 \gamma^2 k_\beta^2 \alpha^2. \tag{23}$$

We have observed x-ray emission due to this betatron motion in our experiments where the beam excuses 1.5 betatron oscillations or 3 oscillations of its envelope.[28] Figure 8(a) shows the total radiated x-ray energy in the 5–30 keV range measured in a cone angle of roughly 10^{-4} radian in the forward direction approximately 40 meters from the exit of the plasma. One can see that the total energy increases as n_p^2 in reasonable agreement with theory. Figure 8(b) shows visible light image produced on a fluorescent paper by the x-rays emitted by the betatron motion (circle at the top) as well by the bending magnet that is used to separate the electron beam from the x-ray photons (the rectangular strip). From the size of the image (~ 4 mm FWHM) one can deduce the divergence angle of the betatron x-rays to be $\sim 10^{-4}$ radian. From the absolute number of x-ray photons at 14.2 KeV measured by precisely tuning the reflecting Si(111) crystal at the Bragg angle we have determined the brightness to be close to 8 $\times 10^{18}$ photons/s/mm^2/sr/0.1% bandwidth.

F. Acceleration and deceleration of beam particles

Now we come to the longitudinal phenomena. In expelling the plasma electrons to form an ion channel, the beam electrons do work and, therefore, must lose energy. If the beam is about half a plasma wavelength long the expelled electrons rush back in and set-up a plasma oscillation which has a longitudinal electric field given by[29]

$$eE = \sqrt{n_p}(\text{eV/m}) \times \frac{n_b}{n_p}\sqrt{2\pi}k_p\sigma_z \frac{e^{-k_p^2\sigma_z^2}}{1 + 1/k_p^2\sigma_r^2}\sin k_p(z - ct). \tag{24}$$

For $k_p\sigma_z \cong \sqrt{2}$, an optimum wake field is excited. The above expression can be simplified in the limit when $eE/m\omega_p c \ll 1$ to

$$(eE)_{\text{linear}} = 240(\text{MeV/m})\left(\frac{N}{4 \times 10^{10}}\right)\left(\frac{0.6\,\text{mm}}{\sigma_z}\right)^2. \tag{25}$$

This is the so-called linear theory[30,31] result which predicts that the longitudinal peak accelerating field scales as $1/\sigma_z^2$ or the beam current divided by the bunch length.

When $n_b > n_p$, the linear theory is no longer valid and one has to resort to particle-in-cell (PIC) code simulations to determine the exact shape and magnitude of the nonlinear wake induced by short, high-current bunches in a plasma.[29] Figure 9 shows an example of such a wake using the code OSIRIS for a $\sigma_z = 100$ μm beam containing 2×10^{10} electrons focused to a 20 μm spot size in a 5.6×10^{15} cm^{-3} plasma. For these parameters the $(eE)_{\text{linear}}$ should be 4.32 GeV/m. Since in the linear theory, the transformer ratio, defined as the ratio of the accelerating field to the decelerating field, is always 2 for a symmetric bunch, the drive bunch slows down at a rate 2.16 GeV/m. The simulations show that
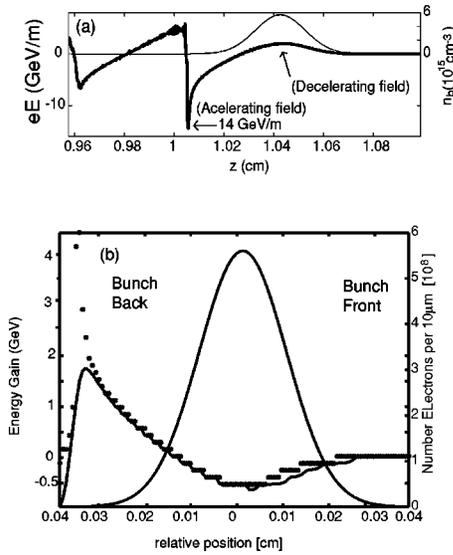
FIG. 9. (a) On axis longitudinal accelerating–decelerating field induced by a $\sigma_z = 0.1$ mm long electron bunch containing 2×10^{10} particles, $\gamma = 60\,000$ in a 5.6×10^{15} cm^{-3} plasma $\varepsilon_N = 50$ mm-mrad and $\sigma_r = 20$ μm. (b) The energy change of the different longitudinal 10 μm long slices of the electron beam (a) after traversing a 30 cm length of the plasma. The largest average energy gain is 1.75 GeV, but some particles gained up to 4.4 GeV. Both (a) and (b) are from 3D, OSIRIS, PIC simulations.

the wake is highly nonlinear with the longitudinal field having a large accelerating spike on axis where the plasma electrons that are expelled by the beam all rush back in to set-up large density spike. The decelerating field is 1.8 GeV/m whereas the peak accelerating field is >14 GeV/m giving a transformer ratio of >7. In the nonlinear regime the wavelength of the plasma wake is reduced and consequently the optimum plasma density is higher than that predicted by the linear theory.

Figure 9(b) shows the energy change that occurs to different longitudinal slices of the beam after traversing just 30 cm of the dense plasma. The bulk of the electrons lose approximately 600 MeV energy whereas the average energy gain of a beam slice approximately 1.2 ps behind the center of the bunch is 1.75 GeV with some particles gaining as much as 4.4 GeV. This simulation shows the potential for achieving extraordinarily high gradients in beam-driven wake field acceleration [known as the plasma wake field acceleration scheme (PWFA)] that were previously thought only possible using intense laser beams interacting with a dense plasma. As we have shown, because it is possible to propagate electron bunches over meter long distances, prospects for obtaining large energy gains using an U-REB driver are extremely likely. In fact, beam and plasma parameters used in the above simulation form the basis of a recently approved PWFA experiment at SLAC known as E164.

Interestingly, even the peak accelerating gradient in this highly nonlinear regime still seems to follow the $1/\sigma_z^2$ scaling law. In Fig. 10 for instance, the 3D PIC simulation result for a $\sigma_z = 40$ μm bunch shows a peak gradient of greater than 40 GeV/m. Such short bunches containing 2×10^{10} electrons have recently become realizable. In fact, the proposed Ultrashort Bunch Facility at SLAC[32] will generate electron
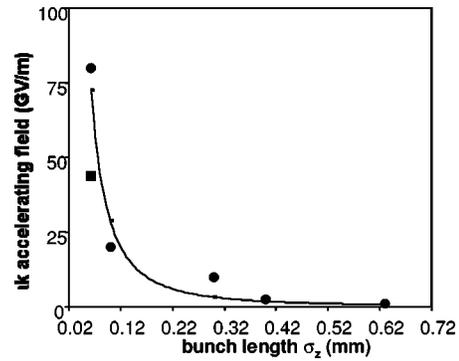

FIG. 10. The peak accelerating field vs the bunch length from PIC simulations and a $1/\sigma_z^2$ fit to the simulations.

bunches that are as short as 30 fs ($\sigma_z = 10$ μm) within a year. Such short bunches lead to extremely high gradients and make feasible an energy doubler[33] experiment using a 50 GeV driver whereby the drive bunch is nearly depleted of its energy in a column of plasma that is just a few meters long while a trailing bunch is accelerated to about twice the drive bunch energy. The issues of emittance preservation and energy spread are being addressed through calculations and simulations for such an "afterburner" for a conventional linear collider.

It should be remarked that wakes generated by an electron beam can also be used to accelerate positrons[34] and muons (μ^+, μ^-). Similarly, the wakes themselves can be produced using positively charged particles although the physics of wake excitation is qualitatively different. As an example consider positron beam induced wakes. When a positron beam enters a quasi-neutral plasma, it attracts plasma electrons from a region that is $\sim c/\omega_p$ wide instead of expelling them as an electron drive bunch would do. There is a spread in the arrival time of these electrons that are being "pulled-in" on axis since they originate at different radii. This phase mixing leads to a lower longitudinal field being excited in the case of a positron driver compared to when an electron bunch is used. Figure 11 compares positron and electron beam excited wakes for identical drive beam parameters which demonstrates this effect. It has been suggested that a positron beam propagating in a hollow channel that is roughly c/ω_p in diameter would lead to an increase in
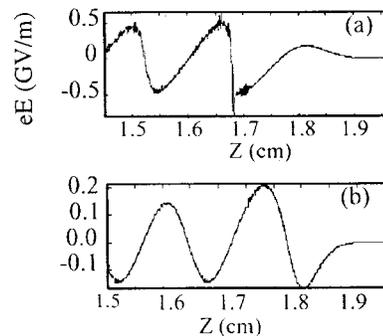

FIG. 11. Comparison of the electron (a) and positron (b) wakes produced in a plasma. $N = 2 \times 10^{10}$, $\sigma_z = 0.4$ mm, $\sigma_r = 75$ μm, $n_p = 4.3 \times 10^{14}$ cm^{-3}. The beams are propagating from the left to the right.

1854   Phys. Plasmas, Vol. 9, No. 5, May 2002
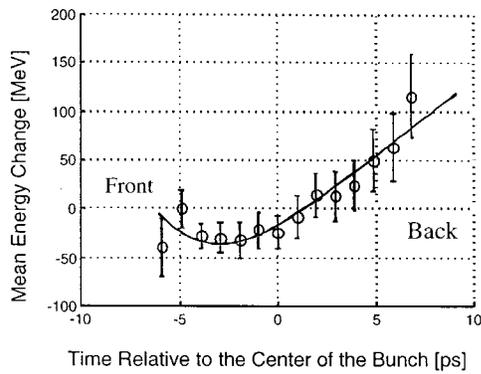
Joshi *et al.*

FIG. 12. A slice-by-slice analysis of the centroid of 1 ps beam slices, showing an indication of energy loss for bulk of the beam and energy gain by the tail particles in the beam.

eE because the positron beam would pull-in electrons from the wall of the channel. Since the electrons now originate at the same radius, their arrival time on axis is the same leading to a larger accelerating gradient.

In the experiments we have studied the energy loss and gain of the beam particles due to the longitudinal dynamics in the plasma using parameters shown in Table III. Time resolved energy spectra were obtained from streak camera images of the beam in the dispersive plane (see Fig. 1) after the FFTB bending magnet. The images are analyzed by slicing the streaks in 1 ps time slices and then the centroid energy of each slice is calculated. Analysis of a typical single event shown in Fig. 12 indicates that the core of the beam has lost about 50 MeV while the electrons in the last slice ($+7$ ps) have gained about 120 MeV. The plasma density for this event was close to the optimum density and the beam exited the plasma after 3 betatron oscillations at a plasma transparency point. It should be noted that because of the space-charge broadening in the streak camera the actual time of these accelerated electrons is somewhat earlier. [In the simulations the maximum energy gain occurs for $\tau = +5$ ps.] In this run an imaging spectrometer was not used to both disperse the electrons and image the exit of the plasma. Although there appeared to be no significant tail on the beam due to the head-to-tail tilt and the data was taken at a plasma transparency point, the streak camera data can be sensitive to transverse motion of the particles. However, we have recently obtained data from a reconfigured experimental set-up which uses an imaging spectrometer to confirm the energy loss of the core and energy gain of the back slices of the beam. The results show that under optimum conditions the beam core can lose up to 170 MeV energy while there is an energy gain exceeding 350 MeV in the tail. These results will be published elsewhere.

IV. CONCLUSIONS

HEDPS with an ultrarelativistic electron beam is seen to be a fertile research area of beam and plasma physics that is relatively unexplored. Some of the physical effects are steering (refraction), focusing, betatron oscillations, emission of spontaneous x-ray radiation due to the betatron motion, and acceleration and deceleration of the beam particles themselves. These phenomena can be theoretically predicted and are seen in full-scale PIC code simulations. There is a good agreement seen between experimental results and theory and simulations. There is promise that HEDPS with U-REBs will affect future accelerator and light source technologies.

[1]E. M. Campbell and M. J. Hogan, Plasma Phys. Controlled Fusion **41**, 39 (1999); M. D. Rosen, Phys. Plasmas **3**, 1803 (1996).

[2]N. Barov, M. Conde, J. B. Rosenzweig, J. B. Schoessow, G. Cox, W. Gai, R. Konecny, J. Power, and J. Simpson, *Proceedings of 1995 Particle Accelerator Conference*, Dallas, TX (IEEE, Piscataway, NJ, 1996), p. 631; J. B. Rosenzweig, B. Briezman, T. Katsouleas, and J. J. Su, Phys. Rev. A **44**, R6189 (1991); T. Katsouleas, S. Wilks, P. Chen, J. M. Dawson, and J. J. Su, Part. Accel. **22**, 81 (1987).

[3]N. Barov, J. B. Rosenzweig, M. E. Conde, W. Gai, and J. G. Power, Phys. Rev. ST Accel. Beams **3**, 011301 (2000).

[4]N. Barov, M. E. Conde, W. Gai, and J. B. Rosenzweig, Phys. Rev. Lett. **80**, 81 (1998).

[5]G. Hairapetian, P. Davis, C. E. Clayton, C. Joshi, S. C. Hartman, and C. Pellegrini, Phys. Rev. Lett. **72**, 2403 (1994); G. Hairapetian, P. Davis, C. E. Clayton, C. Joshi, C. Pellegrini, and T. Katsouleas, Phys. Plasmas **2**, 2555 (1995).

[6]D. A. Hammer and N. Rostoker, Phys. Fluids **13**, 1831 (1970).

[7]M. Hogan, C. E. Clayton, P. Muggli, R. Siemann, and C. Joshi, Phys. Plasmas **7**, 2241 (2000).

[8]P. Muggli, K. A. Marsh, S. Wang, C. E. Clayton, S. Lee, T. C. Katsouleas, and C. Joshi, IEEE Trans. Plasma Sci. **27**, 791 (1999).

[9]P. Catravas, S. Chattopadhyay, E. Esarey *et al.*, Phys. Rev. E **64**, 046502 (2001).

[10]NRL Plasma Formulary, NRL/PV/6790-98-358.

[11]J. D. Lawson, *The Physics of Charged Particle Beams* (Oxford University Press, London, 1988).

[12]S. Humphris, *Charged Particle Beams* (Wiley, New York, 1990); J. L. Cox and W. H. Benett, Phys. Fluids **13**, 182 (1970); W. H. Benett, Phys. Rev. Lett. **45**, 890 (1934).

[13]D. H. Whittum, A. Sessler, and J. M. Dawson, Phys. Rev. Lett. **64**, 2511 (1990).

[14]A. Geraci and D. H. Whittum, Phys. Plasmas **7**, 2241 (2000).

[15]J. S. T. Ng, P. Chen, H. Baldis *et al.*, Phys. Rev. Lett. **87**, 244801 (2001).

[16]J. G. Davis, Ph.D. thesis, University of California, Los Angeles, 1996.

[17]J. B. Rosenzweig and P. Chen, Phys. Rev. D **39**, 2039 (1989).

[18]C. Huang, V. Decyk, S. Wang *et al.*, Bull. Am. Phys. Soc. **46**, 91 (2001).

[19]P. Muggli, S. Lee, T. Katsouleas *et al.*, Nature (London) **411**, 43 (2001); P. Muggli, S. Lee, T. Katsouleas *et al.*, Phys. Rev. ST Accel. Beams **4**, 091301 (2001).

[20]C. Clayton, B. E. Blue, E. S. Dodd *et al.*, "Transverse envelope dynamics of a 28.5 GeV electron beam in a long plasma," Phys. Rev. Lett. (in press).

[21]D. H. Whittum, W. Sharp, S. S. Yu, M. Lampe, and G. Joyce, Phys. Rev. Lett. **67**, 991 (1991).

[22]D. H. Whittum, M. Lampe, G. Joyce, S. P. Slinker, S. S. Yu, and W. M. Sharp, Phys. Rev. A **46**, 6684 (1992).

[23]M. Lampe, G. Joyce, S. P. Slinker, and D. H. Whittum, Phys. Fluids B **5**, 1888 (1993).

[24]K. C. Tzeng, W. B. Mori, and C. D. Decker, Phys. Rev. Lett. **76**, 3332 (1996).

[25]B. Blue, C. E. Clayton, E. Dodd *et al.*, "Test of the electron hose instability in the E157 experiment," *Proceedings of the 2001 Particle Accelerator Conference*, Chicago, IL (IEEE, Piscataway, NJ, in press).

[26] J. D. Jackson, *Classical Electrodynamics* (Wiley, New York, 1975).

[27] E. Esarey, P. Catravas, and W. P. Leemans, *Proceedings of the Advanced Accelerator Concepts 9th Workshop, Santa Fe, NM, 2000*, AIP Conf. Proc. No. 569, edited by P. L. Colestock and S. Kelley (American Institute of Physics, Melville, NY, 2001), p. 473.

[28] S. Wang, C. E. Clayton, B. E. Blue *et al.*, "X-ray emission from betatron motion in a plasma wiggler," Phys. Rev. Lett. (in press).

[29] S. Lee, T. Katsouleas, R. Hemker, and W. B. Mori, Phys. Rev. E **61**, 7014 (2000).

[30] T. Katsouleas, Phys. Rev. A **33**, 2056 (1986).

[31] T. Katsouleas, S. Wilks, P. Chen, J. M. Dawson, and J. J. Su, Part. Accel. **22**, 81 (1987).

[32] P. Emma, R. Iverson, P. Krejcik, P. Raimondi, and J. Safranek, "Femtosecond electron bunch lengths in the SLAC FFTB beamline," *Proceedings of the 2001 Particle Accelerator Conference*, Chicago, IL (IEEE, Piscataway, NJ, in press).

[33] S. Lee, T. Katsouleas, P. Muggli *et al.*, Phys. Rev. ST Accel. Beams **5**, 011001 (2002).

[34] S. Lee, T. Katsouleas, R. G. Hemker, E. S. Dodd, and W. B. Mori, Phys. Rev. E **64**, 045501 (2001).